Molecular Cell
Article

Insights into the Bacterial Transferrin Receptor: The Structure of Transferrin-Binding Protein B from *Actinobacillus pleuropneumoniae*

Trevor F. Moraes,[1,3] Rong-hua Yu,[2] Natalie C.J. Strynadka,[1,*] and Anthony B. Schryvers[2,*]
[1]Department of Biochemistry and Molecular Biology, Center for Blood Research, University of British Columbia, Vancouver, BC V6T 1Z3, Canada
[2]Department of Microbiology and Infectious Diseases, University of Calgary, Calgary, AB T2N 4N1, Canada
[3]Department of Biochemistry, University of Toronto, Toronto, ON M5S 1A8, Canada
*Correspondence: natalie@byron.biochem.ubc.ca (N.C.J.S.), schryver@ucalgary.ca (A.B.S.)
DOI 10.1016/j.molcel.2009.06.029

SUMMARY

Pathogenic bacteria from the *Neisseriaceae* and *Pasteurellacea* families acquire iron directly from the host iron-binding glycoprotein, transferrin (Tf), in a process mediated by surface receptor proteins that directly bind host Tf, extract the iron, and transport it across the outer membrane. The bacterial Tf receptor is comprised of a surface exposed lipoprotein, Tf-binding protein B (TbpB), and an integral outer-membrane protein, Tf-binding protein A (TbpA), both of which are essential for survival in the host. In this study, we report the 1.98 Å resolution structure of TbpB from the porcine pathogen *Actinobacillus pleuropneumoniae*, providing insights into the mechanism of Tf binding and the role of TbpB. A model for the complex of TbpB bound to Tf is proposed. Mutation of a single surface-exposed Phe residue on TbpB within the predicted interface completely abolishes binding to Tf, suggesting that the TbpB N lobe comprises the sole high-affinity binding region for Tf.

INTRODUCTION

In vertebrates, the host iron-binding glycoproteins, transferrin and lactoferrin, play a major role in maintaining an iron-limited environment by sequestering free iron in the extracellular milieu (Ratledge and Dover, 2000). Bacteria are dependent upon effective iron acquisition mechanisms in order to survive in the iron-depleted environment of the host. Pathogenic Gram-negative bacteria within the *Neisseriaceae* and *Pasteurellaceae* families rely on a specialized uptake system, characterized by an essential surface receptor complex that acquires iron from host transferrin (Tf) and transports the iron across the outer membrane (Gray-Owen and Schryvers, 1995).

Actinobacillus pleuropneumoniae is a member of the *Pasteurellaceae* family that causes a highly contagious and frequently fatal form of pneumonia in pigs (Sebunya and Saunders, 1983). Strains of *A. pleuropneumoniae* respond to iron-limiting conditions by expressing surface receptors that are responsible for the pathogen's ability to specifically utilize porcine transferrin (pTf) as a source of iron (Gonzalez et al., 1990, 1995). Both receptor proteins are essential for survival within the porcine lung (Baltes et al., 2002).

Generally, the bacterial Tf receptors are comprised of two proteins: Tf-binding protein A (TbpA) and Tf-binding protein B (TbpB). TbpA is an integral outer-membrane protein related to other well-characterized TonB-dependent receptors involved in the acquisition of siderophore iron or vitamin B12 (Chimento et al., 2003; Fanucci et al., 2003; Ferguson et al., 1998). Its proposed role as the conduit for transport of ferric ions across the outer membrane is supported by the inability of TbpA-defective bacterial strains to grow with Tf as the sole source of iron in vitro (Cornelissen et al., 1992; Irwin et al., 1993) in animal infection models with exogenously supplied human transferrin (hTf) (Renauld-Mongénie et al., 2004) or in the natural host (Baltes et al., 2002; Cornelissen et al., 1998).

TbpB, the second protein component of the receptor, is a surface-exposed lipoprotein that is capable of independently binding Tf (Gray-Owen and Schryvers, 1995; Schryvers and Morris, 1988). The role of TbpB in the iron acquisition process is not fully understood. There is a variable degree of growth impairment in TbpB-deficient strains in vitro where Tf is the sole exogenous source of iron (Anderson et al., 1994; Irwin et al., 1993; Baltes et al., 2002; Renauld-Mongénie et al., 2004). However, TbpB-deficient strains of *A. pleuropneumoniae* are completely avirulent and ineffective at colonization, strongly suggesting that this receptor protein is required for the iron acquisition process in vivo (Baltes et al., 2002). In addition, and in contrast to TbpA, TbpB also has a strong preference for binding to the iron-loaded form of Tf (Retzer et al., 1998; Yu and Schryvers, 1993).

Surface proteins that are essential for survival in the host are of considerable therapeutic interest as potential vaccine targets. The bacterial transferrin receptor, and in particular the largely exposed TbpB component, thus represents such a target, and there have been substantial efforts directed at evaluating and developing TbpB's as vaccine antigens (Danve et al., 1993; Myers et al., 1998; Potter et al., 1999; Rokbi et al., 1997; Rossi-Campos et al., 1992). Preparations of recombinant, refolded TbpB have shown a degree of protection in an aerosol

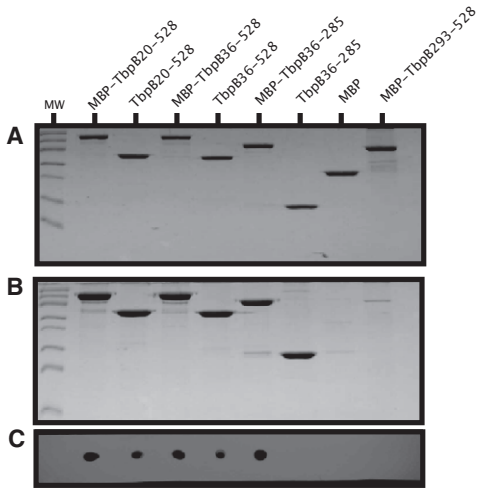

Figure 1. Affinity Capture and Dot Blot Assays Assessing the Function of TbpB Binding to pTf

(A) An SDS-PAGE gel of the purified TbpB proteins used in the pTf-binding assays is shown stained with Coomassie blue.

(B) pTf-Sepharose was used to affinity capture the TbpB proteins in (A). The captured proteins were eluted from resin by SDS-PAGE buffer, separated on a SDS-PAGE, and stained with Coomassie blue.

(C) A direct binding dot blot assay using the proteins in (A) that were spotted on filter paper and probed with HRP-pTf illustrates the binding between pTf and the TbpB proteins.

infection model in pigs (Rossi-Campos et al., 1992). However, there is considerable sequence and antigenic variation among TbpB proteins from different strains of *A. pleuropneumoniae* (Gerlach et al., 1992), prompting the question, how does this protein deal with significant variation yet still bind pTf and function to recruit pTf to the membrane?

Transposon mutagenesis of the *tbpB gene* revealed that TbpB-binding activity for pTf was retained in a fusion protein containing the first 289 amino acids of the mature protein and a series of randomly generated mutants with reduced binding activity primarily mapped to those regions (Strutzberg et al., 1995). A synthetic peptide library representing TbpB from *A. pleuropneumoniae* was probed with labeled pTf to reveal peptide regions with Tf-binding activity (Strutzberg et al., 1997). Similar approaches have been used to probe the tight interactions between TbpB and Tf in several human pathogens (Renauld-Mongénie et al., 1997; Retzer et al., 1999; Sims and Schryvers, 2003), but a clear understanding and appreciation of this interaction has been elusive.

The crystal structure of TbpB described in this study provides significant insight into the molecular role of TbpB as the bacterial receptor of mammalian host Tf and provides the basis for the development of improved TbpB-based vaccines.

RESULTS

Functional Domains of TbpB

Regions encoding various subfragments of the intact *A. pleuropneumoniae* TbpB (residues 1–528) were subcloned into cytoplasmic and periplasmic expression vectors, and the expressed protein subfragments were assessed for Tf-binding activity. The expression vectors encoded N-terminal tag regions containing a consensus biotinylation sequence, a polyhistidine segment, a TEV protease cleavage site, and an optional maltose-binding protein (Mbp) partner. Soluble, stable forms of the Mbp fusion proteins expressed in the cytoplasm could be isolated by metal chelate chromatography (Figure 1A), but only the intact (TbpB$^{20\text{-}528}$ or TbpB$^{36\text{-}528}$) and N lobe (TbpB$^{36\text{-}285}$) subfragments possessed Tf-binding activity as assessed by affinity capture (Figure 1B) or a solid-phase binding activity (Figure 1C). The N lobe subfragments expressed without an Mbp fusion partner, or released by TEV protease cleavage (TbpB$^{36\text{-}285}$, Figure 1), retained Tf-binding activity in the affinity capture assay (Figure 1B) but were negative in the solid-phase binding activity (Figure 1C), highlighting limitations of this assay.

Both the N lobe TbpB$^{36\text{-}285}$ (the smallest subfragment that retained binding activity) and the intact TbpB$^{20\text{-}528}$ (minus the first 19 residues and lipidation site) were selected for crystallization screens. To optimize the isolation of these functional proteins, Mbp fusions to the TbpB constructs were initially captured with an affinity resin consisting of iron-loaded pTf coupled to Sepharose. The fusion protein was eluted from the column with a lower pH buffer containing chelators to favor conversion of the immobilized pTf to the apo form, taking advantage of the specificity of TbpB for the iron-loaded form of pTf. After concentration and buffer exchange, the eluted fusion proteins were shown to retain binding activity by solid-phase binding assays and analytical affinity capture assays (Figure 1). The fusion proteins were treated with TEV protease, yielding a stable TbpB$^{36\text{-}285}$ subfragment or intact TbpB$^{20\text{-}528}$ and the Mbp that could be separated by anion exchange chromatography on a Q-Sepharose column.

Structure Determination of TbpB

The stable N-terminal lobe of TbpB (TbpB$^{36\text{-}285}$) provided the first crystals of a subfragment of TbpB. Selenomethionine-enriched forms of TbpB$^{36\text{-}285}$ crystallized in space group C2, diffracted to 2.3 Å, and provided good phases for structure determination by MAD (Hendrickson et al., 1985) (see Table S1 available online). The intact TbpB$^{20\text{-}528}$ crystallized in similar conditions but in a different space group ($P2_12_12_1$) generating diffraction to 1.98 Å. Using the 2.3 Å TbpB$^{36\text{-}285}$ N lobe structure as a molecular replacement search model, the intact TbpB$^{20\text{-}528}$ structure was solved, yielding an initial R_{fac} of 0.44 with 49% of the model (Table 1).

Structure of TbpB$^{20\text{-}527}$

TbpB adopts a bilobal structure with the two lobes, which we term the N and C lobes, having similar architectures (Figure 2). Each lobe consists of an eight-stranded β barrel flanked by a "handle" domain made up of four (N lobe) or eight (C lobe) β strands. The handle-barrel structured region comprises residues 47–285 of the N lobe and residues 290–528 of the C lobe, indicating that there is an additional long N-terminal peptide region for the N lobe and a very short linker peptide between the two lobes. In the TbpB$^{20\text{-}528}$ structure, the N and C lobes sit orthogonal to one another in an L shape, with the barrel

Table 1. Data Collection and Refinement Statistics for Intact TbpB

	$ApTbpB^{20-528}$
Data Collection	CLS
Space group	P212121
Cell dimensions	
a, b, c (Å)	35.4, 96.8, 143.3
α, β, γ (°)	90, 90, 90
Resolution (Å)	50–1.98 (2.05–1.98)
R_{sym} or R_{merge}	0.092 (0.33)
$I/\sigma I$	24.3 (5.0)
Completeness (%)	98.6 (86.7)
Redundancy	6.7 (5.3)
Refinement	
Resolution (Å)	33.6–1.98
Number of reflections	35,069
R_{work}/R_{free}	0.183/0.225
Number of atoms	4,339
Protein	3,895
Ligand/ion	
Water	444
B factors	21.5
Protein	20.2
Ligand/ion	
Water	24.7
Rmsd	
Bond lengths (Å)	0.007
Bond angles (°)	1.037

Highest-resolution shell is shown in parentheses.

domains on the outer surface and the handle domains in closer proximity (Figure 2A).

N Lobe and C Lobe Structures

The N terminus forms a long unstructured "anchor" region (residues 25–47) that runs along the base of the C lobe barrel into domain A of the N lobe. We term this region the anchor because it is tethered via an N-terminal cysteine that is embedded in the outer membrane through lipidation. Residues 48–130 (domain A) comprise the handle consisting of a four-stranded antiparallel β sheet held together by a short surface-exposed α helix (residues 82–85) (Figure 3A). The four strands in domain A pack up against the N lobe eight-stranded β barrel (residues 131–285) burying ~1800 $Å^2$. Both the eight-stranded β barrel and domain A of the N lobe have extensive loops on a surface-exposed "cap" region and shorter turns on the opposite face that are packed up against two antiparallel strands (an exiting strand β18 that links N lobe to C lobe and the strand β8 that connects the handle and β barrel of N lobe) (Figure 2).

The similarity in architecture between the N and C lobes of TbpB is supported by an overall root-mean-square deviation (rmsd) of 2.0 Å (aligning 160 C-alpha atoms). The primary difference is located in the handle domains (A and C) with an rmsd of 2.7 Å (aligning 61 C-alpha atoms). The handle domain of the C lobe (domain C) consists of a squashed six-stranded β sheet flanked by two antiparallel β strands and has no supporting α helix as in the N lobe (Figure 3B). The six strands pack against the β barrel domain of C lobe burying 2100 $Å^2$ of surface area. Structural overlays illustrate the differences in the loop and helix regions of these supporting handle structures (Figure 3C). The strands of the β barrel domains within the N and C lobes are superimposable, with an rmsd of 1.8 Å (aligning 107 C-alphas); however, the loop regions are quite distinct, especially the first loops created within the β barrels. As with many β barrels, short turns extend on the vertex side of the β barrel domain, and large extended loop regions exist on the surface-exposed cap region of C lobe (Figure 3B).

These long flexible loop regions contribute to quite different electrostatic surfaces; N lobe has a positive potential centered at its cap region, whereas C lobe's cap region is negatively charged and creates a visible cavity between its two domains (Figures 3D and 3E). The difference in electrostatic potential may contribute to the distinct binding properties of N and C lobe. Indeed, the Tf-binding affinity for N lobe is much greater than C lobe, as can been seen in pTf affinity capture and solid-phase binding assays (Figure 1). In addition, ITC data confirm that the affinity for Tf must come primarily from the N lobe, as the K_d for N lobe ($TbpB^{36-285}$) and intact TbpB ($TbpB^{20-528}$) are almost equivalent at 35 and 44 nM, respectively (Figure S1). The 1:1 stoichiometry between pTf and N lobe or intact TbpB was also supported by multiangle light scattering (MALS; data not shown).

The Interface between N and C Lobes

The interface between the N- and C-terminal lobes buries ~1200 $Å^2$ of surface area and contains a central hydrophobic core consisting of residues Ile294, Ile295, and Phe313 from C lobe, and Pro45, Leu47, and Pro129 from N lobe. This hydrophobic core is flanked by salt bridges formed by Glu309-Lys131 and Arg293-Asp296 (Figure 4). In addition, Lys325 forms a hydrogen bond with the peptide backbone hydroxyl of Pro45, and the aliphatic portion of Asn311 engages in van der Waals contacts with Leu47 and Pro129. Residues in the C/N lobe interface are absolutely conserved in porcine pathogens (Figures S2 and S3) and are highly conserved in all TbpBs (Figure S4).

Furthermore, the N-terminal region (specifically residues 26–29, 31, and 34) of the intact $TbpB^{20-528}$ structure stacks against the overhanging eighth strand of the C terminus of C lobe (residues 524–527). Most contacts are through the main chain, as the nature of the interaction is a short antiparallel β strand, with the side chains of the interacting residues still partially conserved in TbpB (Figures S3 and S4). No other portion of the subsequent long flexible unstructured N-terminal region (residues 35–42) makes contact with the C lobe.

Interactions of TbpB with Tf

A combination of modeling and site-directed mutagenesis was used to probe the TbpB-Tf interaction. Since our binding studies suggest Tf-binding activity primarily resides in the TbpB N lobe (Figure 1) and interactions are thought to primarily involve the C lobe of Tf (Alcantara et al., 1993), we attempted to generate a model of the C lobe pTf bound to the N lobe of TbpB. Using

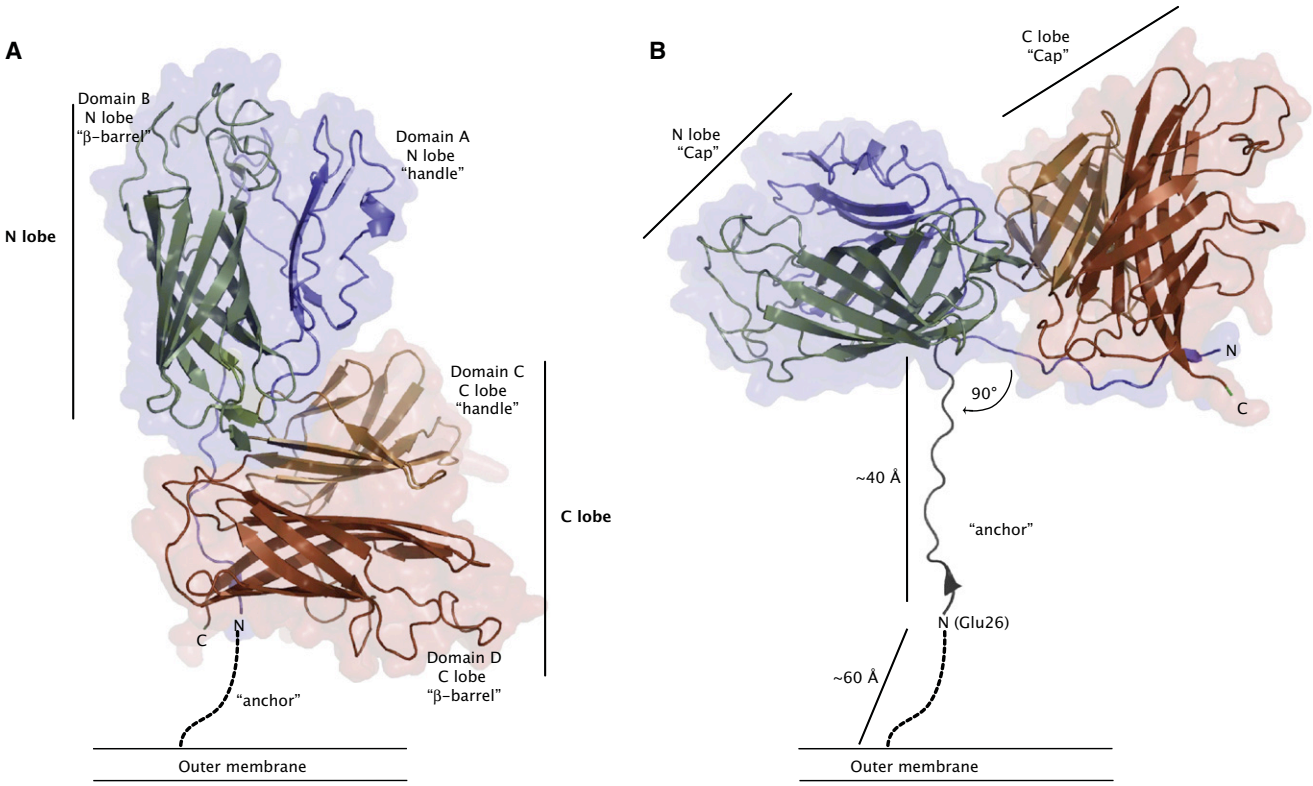

Figure 2. Overall Structure of TbpB

Illustrated is a cartoon representation of TbpB with domains A–D labeled and colored teal, green, gold, and orange. The N lobe and C lobe are labeled and highlighted with a blue and red semitransparent surface.

(A) The C- and N-terminal positions of the protein are labeled, and the lipidated cysteine of mature protein is modeled tethered with respect to the outer membrane.

(B) An alternate hypothetical model of TbpB extending from the membrane and reliant on eliminating the interactions between the N- and C-terminal strands. The anchoring residues are rotated 90° around the peptide bond at residue 42.

PyMOL (DeLano, 2002) to orient the C lobe of Tf to within 30 Å of the N lobe cap region, both proteins were randomly spun around their center of mass and docked using RosettaDock from the ROSETTA++ Software Suite (Gray et al., 2003). One thousand decoys of N lobe TbpB bound to C lobe pTf were generated, and the ten lowest-energy models were superimposable (Figure 5 and Figure S5). The docked model places the C1 and C2 domains of pTf above the barrel and handle domains of TbpB N lobe, respectively.

Based on the model generated by Rosetta, we examined key surface-exposed residues of N lobe for pTf binding. Two hydrophobic surface-exposed residues, Phe171 (located on loop X of the N lobe barrel) and Phe58 (located on a loop in the N lobe handle domain), flank an electropositive patch on the cap region of N lobe (Figure 6A). These residues were targeted for site-directed mutagenesis along with "control" surface residues, Ala83, Asn84, and Ser86, not anticipated to play as critical a role in pTf binding. The resulting mutant Mbp-TbpB N lobe fusion proteins (Phe58Glu+Lys61Glu, Ala83Glu, and Phe171Ala) were produced and tested for binding by affinity capture, solid-phase binding assays, and ITC (Figures 6B–6D and Figure S1). Mutation of Phe171 abrogated binding of pTf completely, whereas binding activity was reduced for the simultaneous mutation of Phe58 and Lys61 from 55 to 309 nM as measured by ITC (Figure 6D and Figure S1). As predicted from the model, the control surface mutations Asn84Arg and Ser86Glu had no negative effect on pTf association in affinity capture or solid-phase binding assays (data not shown), nor did Ala83Glu (Figures 6B–6D).

DISCUSSION

Structural Features of TbpB and Its Interface with Tf

This study presents the structural report of a bacterial receptor protein responsible for binding Tf from the infected host. The bilobed structure of TbpB is orthogonal in architecture with reference to the positions of the N and C lobes. It is tempting to speculate that the bilobal structure of TbpB would interact with the bilobal structure of Tf, lobe to lobe. Although the overall folds of the N and C lobes are similar, the differences in the handle domains and loop regions (we term the cap) lead to very different morphologies and electrostatic binding surfaces. This cap region on the N lobe is highly electropositive, whereas the equivalent cap region of the C lobe forms a deep electronegative gorge between the handle and β barrel domains (Figures 3D and 3E), differences we propose govern binding to Tf. Furthermore, we show the TbpB N lobe has similar affinity for

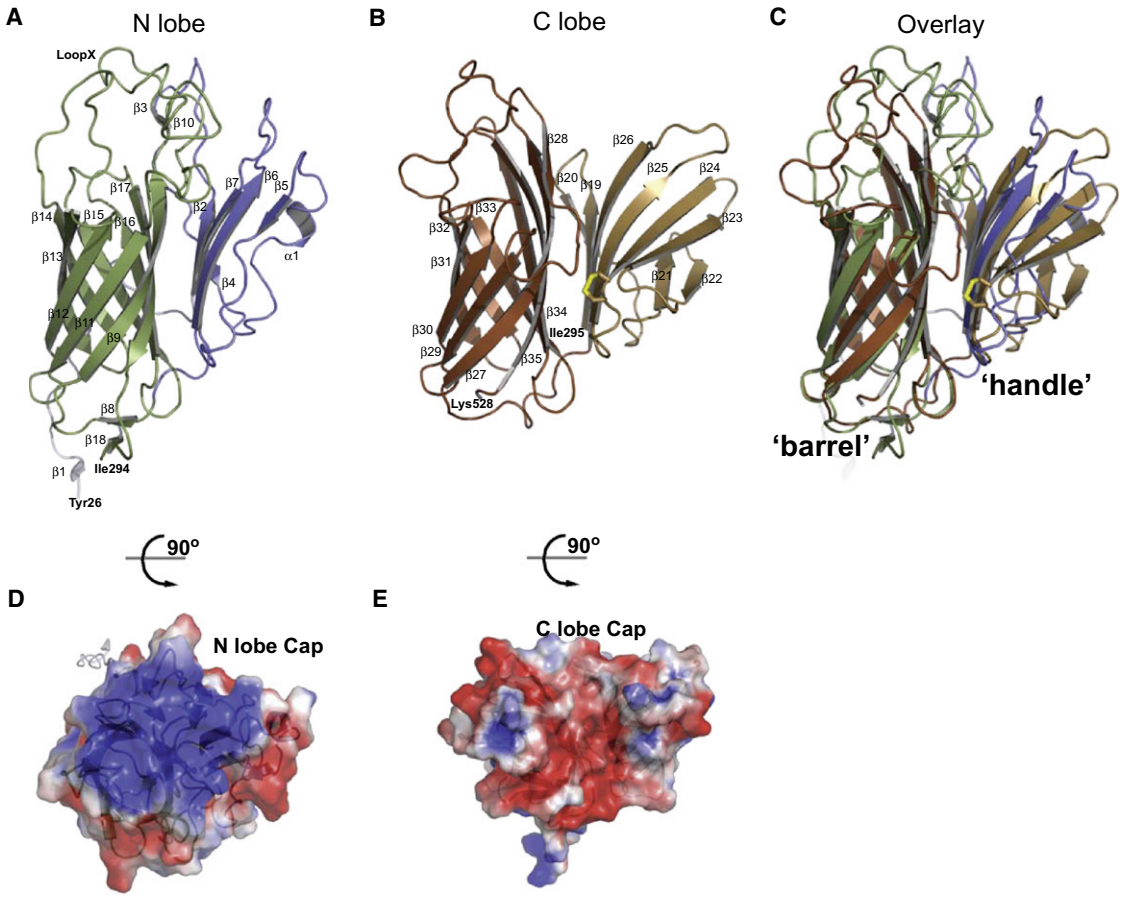

Figure 3. N Lobe and C Lobe of TbpB

(A and B) (A) A cartoon representation of TbpB N lobe residues 47–284 and (B) C lobe residues 290–526. The terminal residue numbers, helices, and strands are labeled.

(C) Superposition of TbpB N and C lobes using SSM in Coot. The secondary structural elements are labeled.

(D and E) (D) The electrostatic surface potential as calculated by APBS in Pymol is illustrated for N lobe and (E) C lobe.

iron-loaded pTf as full-length TbpB, whereas C lobe has no significant affinity for pTf (Figures 1 and 5, Figure S1). Taken together, it seems unlikely that the C lobe functions to bind Tf in the same manner as the N lobe.

The lack of structural information for TbpB has limited the design and interpretation of prior studies exploring the interaction between TbpB and Tf. With the high-resolution structures of TbpB and Tf now in hand, a combination of molecular docking,

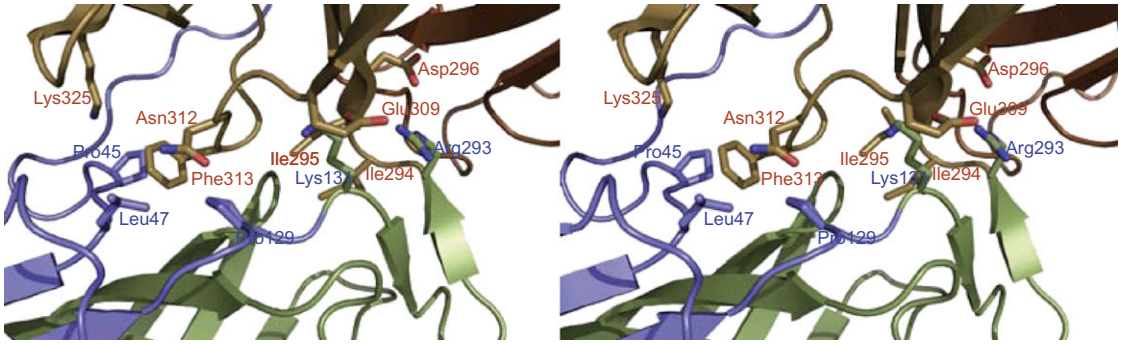

Figure 4. Interface between N and C Lobes of TbpB

The interface between the N and C lobes of TbpB is shown in a cross-eyed stereoimage. Domain A and B from N lobe are colored blue and green, respectively, and domain C from C lobe is colored brown. Residues in the interface are labeled.

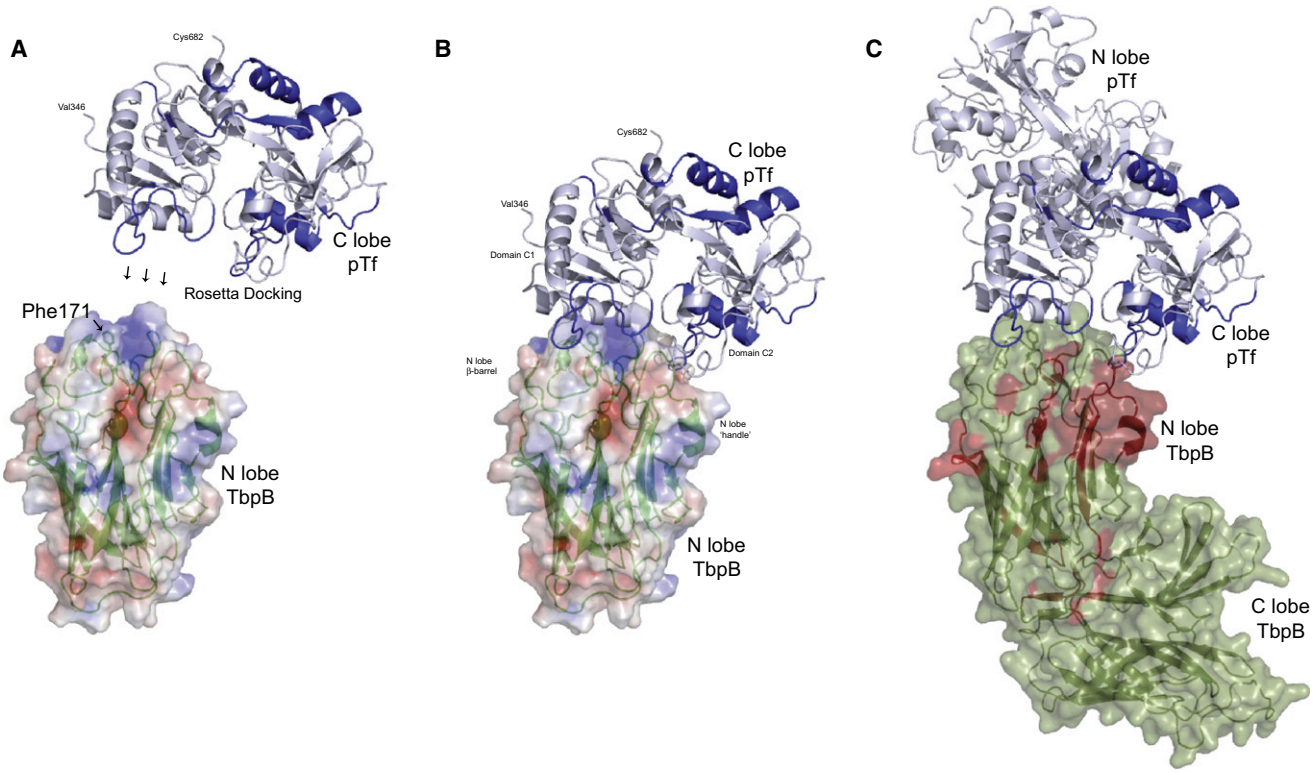

Figure 5. Rosetta-Docked Model of TbpB-Bound pTf

The N lobe of TbpB and the C lobe of pTf (holo) (PDB ID code 1H76) were docked together using the Rosetta suite for protein docking. One thousand models were generated, and the top ten lowest energy models were superimposed (Figure S5).

(A) The electrostatic surface of TbpB N lobe (generated by ABPS and PyMOL using default parameters; ionic strength set at 0.01 and neutral pH) is shown along with a cartoon of the holo-C lobe of pTf colored white, with binding determinants from the peptide arrays colored in blue.

(B) The C lobe of pTf docked onto N lobe TbpB.

(C) The subsequent model illustrating the position of the proposed complex pTf (ribbon) bound to TbpB (transparent surface). The surface illustrating *A. pleuropneumoniae* TbpB-binding determinants are colored in red.

site-directed mutagenesis, ITC, and functional assays were used to probe and model the TbpB-Tf interface (Figure 5). Collectively, these data suggest that the interface is localized to the distinctive cap region of TbpB N lobe described above and provides the foundation for both understanding past work as well as ultimately understanding the role and specificity of TbpB in iron acquisition from host Tf.

Within the context of our structural data, the majority of point mutants previously characterized in *A. pleuropneumoniae* TbpB to impair pTf binding (Strutzberg et al., 1995) are either not surface exposed or in a region that would lead to detrimental folding. As such, it is unlikely that any of these mutants are defective due to a direct binding interaction with pTf. For example, the Gly205Asp mutation that caused a severe loss of binding is located within β strand 12 of the N lobe β barrel (Figure 7A). This would direct the charged Asp into the hydrophobic interior of the N lobe in order to maintain the antiparallel β strands that form the N lobe β barrel, thus likely abrogating proper folding.

In contrast, in this study we have designed and probed, using mutagenesis, the surface-exposed residues located at the interface of our predicted model of TbpB bound to pTf. The Phe171Ala mutation located at the center of the interface completely abolished Tf binding, whereas the double mutant Phe58Ala and Lys61Glu involving residues located on the edge of the interface also had an effect on pTf binding (Figure 6). Mutating another surface-exposed residue that was not in the interface, Ala83Glu, for example, had no effect on binding.

A common approach for dissecting protein/protein interactions in lieu of structural data involves peptide mapping. Three regions of the *A. pleuropneumoniae* TbpB N lobe were previously identified as potential binding sites for pTf by probing an overlapping synthetic peptide library with labeled pTf (Strutzberg et al., 1995). Now interpreted within the context of our structural data, the first region represented by residues 121–134 is buried in the interface between domain A and the N lobe barrel and is unlikely to be involved in pTf binding, as it would require energetically and sterically unfavorable conformational changes to separate the barrel and handle domains. Thus this region likely represents a false positive that is an inherent limitation of the peptide library approach. The second region represented by residues 81–94 encompasses the surface-exposed helix region within domain A of our structure. However, our mutagenesis analysis of surface-exposed residues in this region (Ala83Glu) indicated that pTf binding was not affected. In addition, the

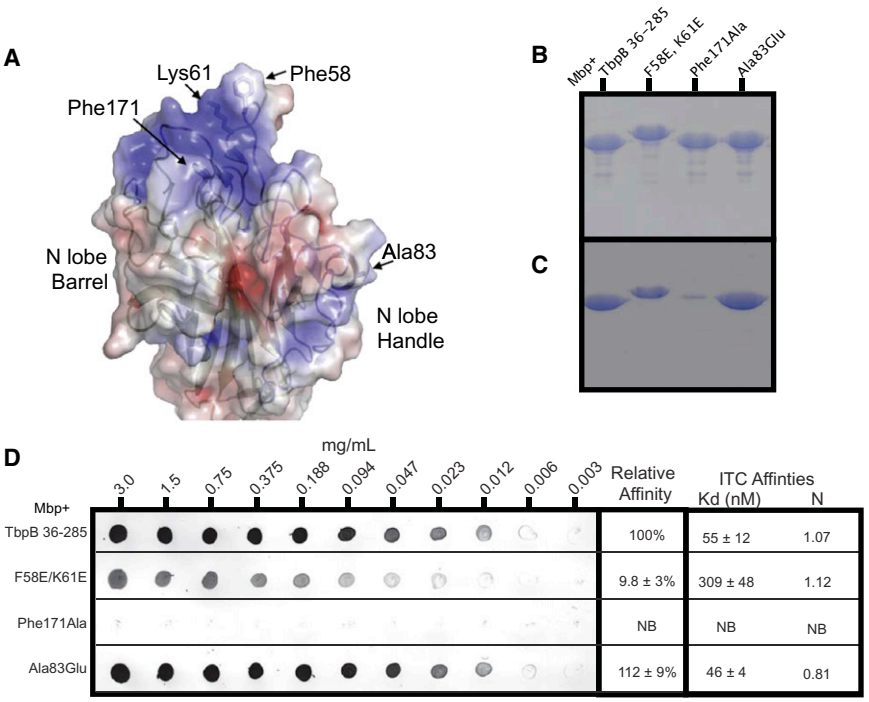

Figure 6. Potential pTf-Binding Residues

(A) Surface-exposed residues Phe58, Lys61, Ala83, and Phe171 are illustrated on an electrostatic semitransparent surface of the N lobe cap.

(B) An SDS-PAGE gel of NiNTA purified His-Mbp-TbpB N lobe protein and mutants, Phe171Ala, Phe58Ala-Lys61Glu (K58E, K61E), and Ala83Glu, stained with Coomassie blue.

(C) pTf-Sepharose was used to capture the TbpB proteins in (B). The captured proteins eluted from the resin by SDS-PAGE buffer were separated on an SDS-PAGE gel and stained with Coomassie blue.

(D) Varying concentrations of His-Mbp-TbpB N lobe constructs were spotted on filter paper and probed with HRP-pTf. The blots were scanned and quantified to give a saturated binding curve, and relative binding constants were determined by Scatchard analysis with respect to the His-Mbp-TbpB$^{35-285}$(N lobe). Binding constants for pTf bound to the His-Mbp-TbpB constructs were also determined by ITC and listed (isotherms can be found in Figures S1C and S1D).

underlying sequence in this region is not highly conserved even within serotypes of *A. pleuropneumoniae* (Figures S2 and S3). Only the third region predicted by the peptide studies, specifically residues 162–174, encompasses an area compatible with pTf binding in our structure: loop X on the cap of the barrel of N lobe between strands β9 and β11. This loop region is surface exposed in our structure, creates a distinguishing highly electropositive surface, and includes Phe171, for which involvement in pTf binding has been supported by our site-directed mutagenesis analysis.

TbpB Conservation and Implications for Vaccine Design

An overall sequence comparison of TbpBs from a variety of species that infect different vertebrate hosts (Figure S4) highlights the predicted conservation of the secondary structural elements, suggesting that they share the same overall architecture. The greatest conservation appears to be in the strands of the β barrel and handle domains, especially those residues within the interface between the handle and β barrel. The loop regions that comprise the interface between N and C lobe are also highly conserved, signifying either that this interaction is

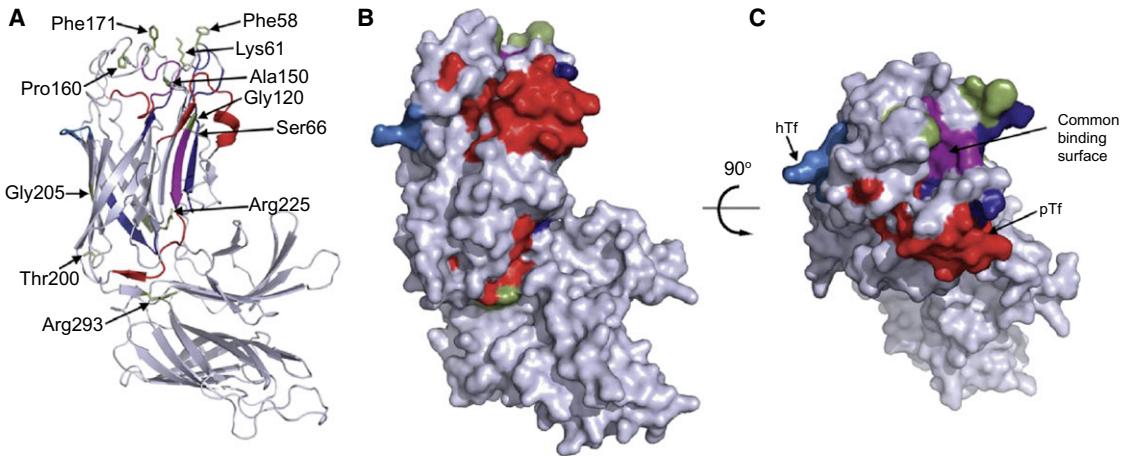

Figure 7. TbpB-Binding Determinants for Tf Mapped on the Structure of *A. pleuropneumoniae* TbpB

A ribbon (A) and two surface (B and C) representations of TbpB. Peptides identified from a peptide library of *A. pleuropneumoniae* TbpB that bind to pTf are colored in red, and residues that inhibit the interaction between *A. pleuropneumoniae* TbpB and pTf are labeled and colored in green. Highlighted in blue are the equivalent positions of peptides involved in interactions between hTf and *Neisseria meningitidis* B6B16 (light blue) or *Moraxella catarrhalis* (dark blue). Common binding regions to pTf or hTf binding found in TbpBs are highlighted in purple.

conserved or that they mediate conserved interactions with other outer-membrane components. The difference in size among the TbpBs is primarily due to additional sequences within the handle domains.

The structural information provided by this investigation can also be used to aid interpretation of experimental data regarding interactions between hTf and TbpBs from human pathogens, and two studies in particular provide substantial insights. In the first study, site-directed mutagenesis of an isotype 2 TbpB from *N. meningitidis* was used to identify two Arg residues from the N lobe that are critical for interaction with hTf (Renauld-Mongénie et al., 2004) (Figure 7). Arg243 from *N. meningitidis* localizes onto an extended loop between β strands 12 and 13 that is common in sequence among hTf-binding TbpBs and may be specific for recognition for hTf. Arg55 from *N. meningitidis* maps to the handle domain of the N lobe cap near Phe58 and Lys61 in *A. pleuropneumoniae* TbpB, which have been shown to moderately effect pTf binding.

In perhaps the most comprehensive study, peptide libraries and truncations of the TbpB N lobe from the human pathogen *Moraxella catarrhalis* probed with hTf identified six regions involved in hTf binding (Sims and Schryvers, 2003), with several of the peptides mapping to the N lobe cap region of TbpB (Figure 7C). Taken together, these studies investigating the interactions between hTf and the human bacterial pathogens *N. meningitidis* or *M. catarrhalis* support the general interface between TbpB and Tf we have modeled for the *A. pleuropneumoniae* TbpB-pTf interaction.

Alignment of TbpB sequences from porcine pathogens (Figures S2 and S3) as well as other vertebrate pathogens (Figure S4) illustrates that, in spite of overall sequence and predicted fold conservation, a considerable portion of the surface of the N lobe is comprised of variable sequence. This variability primarily resides in the "cap" loop regions within the N lobe and we predict reflects, in part, the fact that Tf receptors from distinct pathogens have evolved to recognize the Tf of their specific infected host. However, comparison of sequences from porcine pathogens that would bind a common pTf still show a concentration of variable sequence at the N lobe cap (this is also observed between serotypes of *Neisseria meningitidis* B16B6 and M982, Figure S4), an effect we believe is caused by selective pressure from the host immune system (Figures S2 and S3). Of the 40 highly exposed surface residues in N lobe, only seven are conserved among the various *Actinobacillus pleuropneumoniae* and *Haemophilus parasuis* serotypes. Similar to the *Neisseria gonorrhoeae* type IV pilus system, where pilin subunit regions that are most accessible to antibodies are also the most variable (Craig et al., 2006), regions of TbpB located on the surface-exposed cap region are hypervariable, whereas the buried β strands in the core of the structural fold are more highly conserved (Figures S2–S4). In contrast, the surface residues of the TbpB C lobe are highly conserved, implying less selective pressure from the immune system and ostensibly less exposure than N lobe at the bacterial membrane. We speculate the C lobe of TbpB may function as a scaffolding region that is bound by other proteins (including TbpA) to effectively mask the TbpB surface and protect it from eliciting an immune response prior to the Tf capture event. Together this information provides the platform toward the design of vaccines that could be exploited as therapeutic agents.

Structural Homologs and Functional Homologs of TbpB

The overall architecture of TbpB defined in our crystal structure is unique; however, each domain falls into a structural fold. Based on a Dali search, the eight-stranded barrel domains in N and C lobe draw comparisons to eight-stranded β barrel outer-membrane protein W (OmpW). These eight-stranded integral outer-membrane proteins utilize hydrophobic residues lining the outer surface of the β barrels to create an apolar membrane-spanning region with an internal polar cavity for transport of molecules. This is opposite to the barrel domains of TbpB (Figure 2), where the hydrophobic residues line the inner surface of the β barrels to create a stable hydrophobic core.

The barrel domains of both the N and the C lobe also share structural homology with two other recently characterized surface-exposed lipoproteins, LP2086 (Mascioni et al., 2008) and GNA1870 (Cantini et al., 2006, 2009; and Schneider et al., 2009). GNA1870 is a 28 kDa surface-exposed lipoprotein of *Neisseria meningitidis* (Cantini et al., 2006). The protein is a meningococcal vaccine candidate that binds the complement regulatory protein factor H and is thus also known as factor H-binding protein (FHbp) (Madico et al., 2006). The NMR structure of a domain of truncated FHbp ($FHbp^{101-255}$; Protein Data Bank [PDB] ID code 1YS5) forms an eight-stranded β barrel that can be overlayed onto TbpB N lobe (rmsd of 2.3 Å over 84 common main-chain atoms) or C lobe (rmsd of 3.3 Å over 60 common main-chains atoms) (Figure S6). Despite the similarities in the β barrel domain of FHbp and TbpB, however, the loop regions and handle domains are distinct, and neither supports the affinity for each other's substrates (Cantini et al., 2006). Furthermore, an overlay with the recent crystal structure of FHbp bound to compliment factor H implicates a completely different binding surface that employs the wedge created between the handle and barrel β strands and not the barrel cap regions we predict for TbpB-Tf (Figure S6). These comparisons thus suggest that surface-exposed lipoproteins like TbpB and FHbp may employ a common fold for purposes of secretion or stability, but not for ultimate unique function at the bacterial membrane.

Despite serving the same function, to obtain iron from Tf, the prokaryotic and eukaryotic Tf receptors are quite dissimilar both in structure and function. The prokaryotic Tf receptor is comprised of two structurally different components (TbpA and TbpB), whereas the eukaryotic receptor is a homodimeric ectodomain (Lawrence et al., 1999; Cheng et al., 2004) (Figure S7). The ectodomains allow mammalian cells to effectively bind and utilize any iron-loaded Tf from a mammalian species as an iron source, whereas the prokaryotic Tf receptor is exquisitely specific for Tf from the host it infects. Finally, the prokaryotic receptor removes iron from Tf at the cell surface and transports it across the outer membrane, whereas the eukaryotic Tf receptor complex is "internalized" via endocytosis and the lower pH of the endosome plays a major role in recovering the iron from Tf. The structural and functional differences between the TbpA/TbpB Tf receptor and the ectodomain further emphasize the

potential for TbpA and TbpB to serve as ideal bacterial vaccine candidates.

Additional Functional Implications

TbpB serves to preferentially capture iron-loaded (holo) Tf at the extracellular surface of the bacterial outer membrane, then ostensibly releases apo Tf once iron is extruded into the bacterial cell. In addition to the predicted TbpB-Tf interface, our structural analysis may provide additional insight into these processes. During the initial recruitment of host Tf by TbpBs, we suggest the unstructured N-terminal region following the lipidation site we observe in TbpB may serve to provide a flexible tether to the membrane surface. By analogy with observed multiple conformations of a similar N-terminal region in the NMR-derived model of the surface lipoprotein LP2086 (PDB ID code 2KDY) (Mascioni et al., 2008), it is tempting to speculate that similar rotations around the peptide bond between residues 42 and 43 in TbpB would allow the receptor to extend a further 40–60 Å from the bacterial cell surface to capture Tf from the extracellular milieu. This modeled alternate orientation is consistent with the overall structural features, and one might suggest that the energetic cost required for the necessary elimination of the three hydrogen bond interactions between the N-terminal anchor and the C lobe during this reorientation (Figure 2B) may be compensated for by the favorable binding with Tf.

The structural model for pTf-TbpB that we present here also reconciles the strong preference of TbpB for the iron-loaded form of Tf (Retzer et al., 1998). A substantial 50° rotation was observed between the C1 and C2 domains of Tf upon interconversion between the apo and iron-loaded forms (Rawas et al., 1997). This rotation would result in an ~13 Å displacement of the equivalent C lobe pTf residues (C1-His353 and C2-Asp558) we predict to lie at the interface with TbpB. Superposition of the apo and iron-loaded forms of Tf onto our Rosetta-modeled complex suggests that the cleft created between the C1 and C2 domains as iron is extracted to create apo-Tf and would require an energetically unfavorable disruption of the bound TbpB handle-barrel domains, thus resulting in TbpB's reduced affinity for apo-Tf. Interestingly, our modeling studies also suggest that a better fit between TbpB and iron-loaded pTf could be envisioned with only a small movement of a helix in domain C1 of Tf further into the electropositive groove within the N lobe cap of TbpB. It is tempting to speculate that this type of induced conformational destabilization upon TbpB binding may serve as an important initial step in lowering the affinity of Tf for iron. TbpB's primary role is to bind and recruit Tf to the bacterial membrane, but it may also function to help lower Tf's affinity for iron, thereby increasing the efficiency of subsequent iron uptake by the bacterial cell.

EXPERIMENTAL PROCEDURES

Preparation of pTf-Sepharose and HRP-pTF

Porcine transferrin (pTf), obtained from Sigma-Aldrich, was conjugated to CNBr-activated Sepharose 4B (Pharmacia). Briefly, 5 mg of pTf was incubated with 1 g of CNBr-activated Sepharose 4B for 2 hr in coupling buffer (0.1 M $NaHCO_3$ [pH 8.3], 0.5 M NaCl) followed by washing overnight with 50 mM Tris (pH 8.0), 1 mM ethanolamine-HCl. The pTf-Sepharose resin was incubated for 10 min in 0.1 M sodium citrate/0.1 M sodium carbonate (pH 8.6) buffer in the presence of 25-fold molar excess of $FeCl_3$. Iron-pTf-Sepharose was washed with 10 mM HEPES (pH 7.0) and stored at 4°C.

The HRP conjugate of pTf (HRP-pTF) was prepared as previously described (Gonzalez et al., 1990). Briefly, after chemical conjugation, the mixture of HRP and pTf was loaded onto a Superdex 200, and the fraction from the peak corresponding to a 1:1 conjugate was pooled and dialysed against PBS, and aliquots were frozen and stored at −80°C.

Expression and Purification of Recombinant TbpB

Plasmids containing the *A. pleuropneumoniae* TbpB constructs were transformed into *E. coli* ER2566 chemically competent cells (NEB Company) and left to recover in 1 ml LB for 1 hr at 37°C. LB (20 ml) containing 100 μg/mL ampicillin was added to the transformants and grown at 37°C overnight with shaking. The 20 ml overnight cultures were used to inoculate 4.5 L of LB broth with 100 μg/mL ampicillin and left shaking O/N at 37°C. Cells were harvested at 4600 × g and resuspended in 100 ml of lysis buffer (50 mM Tris-HCl [pH 8.0], 1 M NaCl) containing phenylmethylsulfonyl fluoride (PMSF) (1 mM). Cells were lysed by passage through a french press cell at 10,000 psi twice. Cell debris was removed by centrifugation at 10,000 × g for 30 min. The supernatant was incubated with 25 ml iron-pTf-Sepharose resin in a 500 ml bottle and left shaking overnight at 4°C. The resin was collected by a 25 ml gravity filter column and washed ten times in lysis buffer. The bound receptor protein was eluted with an iron removal buffer (0.1 M sodium phosphate, 0.1 M sodium acetate, 10 mM EDTA [pH 5.5]). The eluted sample was dialyzed against 10 mM HEPES (pH 7.0) at 4°C for overnight with two changes of 2 L. After dialysis, the protein solution was analyzed by SDS-PAGE. The pure protein was concentrated to a final volume of 5–10 ml and stored at 20°C.

Direct Binding Dot Blot Assay

Protein samples were spotted onto nitrocellulose/cellulose acetate membrane (0.45 micron, HA paper; Millipore Ltd.). After drying at room temperature, nonspecific sites were blocked by incubating with 0.5% skim milk in TBS (50 mM Tris-HCl [pH 7.4], 150 mM NaCl) for 10 min at room temperature under gentle agitation. The membrane was washed with TBS (20 mL, three times) and then incubated with HRP-pTf (1:2000) in TBS with 0.5% skim milk for 1 hr at room temperature under gentle agitation. The membrane was washed with TBS followed by a 15 min incubation in a developing solution (20 ml TBS, 150 μl 3% H_2O_2, and 4 ml of 300 mg chloronaphthol [Bio-Rad HRP reagent] in 100 ml cold methanol). After sufficient time for the spots to develop, the membrane was washed with water and dried at room temperature.

Small Batch Isolation of *A. pleuropneumoniae* TbpB Using pTf-Sepharose

Sample protein (~0.05 mg/mL) was incubated with 50 μl iron-pTf-Sepharose for 1 hr at room temperature under gentle agitation. After collecting the resin by centrifugation, the resin was washed three times with 50 mM Tris/HCl (pH 8.0) containing 1 M NaCl to remove contaminants. The resin was boiled for 5 min in the presence of 2× sample buffer (4% SDS, 20% glycerol, 0.002% bromophenol blue in 100 mM Tris/HCl buffer [pH 6.8]), and the bound TbpB protein was visualized on 13.5% SDS-PAGE gels stained with Coomassie blue.

TEV Cleavage Method

Pure fusion protein was digested with TEV protease (4 mg /100 units) in TEV buffer (50 mM Tris-HCl [pH 8.0], 0.5 mM EDTA) at room temperature overnight. After cleavage, the protein solution was dialyzed against 10 mM HEPES (pH 7.0) at 4°C overnight and then applied in batch to 20 ml of Q-Sepharose resin (equilibrated in 10 mM HEPES [pH 7.0]). The flowthrough and bound protein were analyzed by SDS-PAGE, and pure protein was concentrated and stored at 4°C or −20°C.

Protein Crystallization

Purified $TbpB^{36-285}$ protein at 10, 20, and 30 mg/mL was initially screened against QIAGEN PEG suite commercial screen with a 32-head Honeybee robot at the University of Alberta. Initial crystals were observed in 150 mM potassium thiocyanate and 30% PEG 2000 MME. The addition of 20% glycerol yielded a C2 isoform. $TbpB^{20-528}$ (intact TbpB) crystallized in similar conditions that were optimized to 20% PEG3350, 0.1M Tris (pH 8.0), 150 mM NaCl in $P2_12_12_1$.

Structure Determination

Data were gathered on crystals frozen at 105 K on beamline ID08-1 at the CLS. The anomalous peak, high-energy remote, and inflection wavelengths for selenomethionine-enriched $TbpB^{36-285}$ crystals were determined by a fluorescence scan; subsequently, 360 images, 180 images, and 180 images with 1° oscillations were collected at the corresponding energies (Table 1). The data were processed with HKL2000 (Otwinowski and Minor, 1997) anomalous flag to 2.3 Å resolution. The position of three Se atoms was determined and refined by Sharp (Vonrhein et al., 2007) using Shelx for HA detection and Solomon for density modification. ArpWarp (Morris et al., 2002) was used to build an initial model consisting of 212 docked residues, providing 43% of the model. Further rounds of model building and refinement were completed by using Coot and Refmac5 (Murshudov et al., 1997) utilizing TLS (Winn et al., 2001) parameters and the Phenix suite. $TbpB^{20-528}$ crystals were soaked in 30% PEG3350, 0.1 M Tris (pH 8.0), 150 mM NaCl and flash frozen in liquid nitrogen. Data sets collected on beamline ID08-1 at the CLS were processed with HKL2000. The 2.3 Å resolution $TbpB^{36-285}$ N lobe structure was used as a molecular replacement search model in MOLREP yielding an initial R_{fac} of 0.44 with 50% of the model for the $TbpB^{20-528}$ structure. The first six amino-terminal residues of $TbpB^{20-528}$ are poorly defined in the electron density maps and are not modeled. Residues are numbered initiating with the first mature amino acid (Cys1) remaining after signal peptide cleavage. Weak density was observed for several side chains of residues (366–371 and 474–480). There were no disallowed residues in the Ramachandran plot (4.5% allowed). Figures were made using PyMOL (DeLano, 2002). Electrostatic potentials were calculated using APBS (Baker et al., 2001) under default parameters (Protein Dielectric, 2.0; Solvent Dielectric, 80.0) at neutral pH (all charged ion concentrations set to 0). No observable differences in potential were observed at an ionic strength of 150 mM for the ±1 ion concentrations. Maps were contoured at ±4 kT/e for isosurface display.

Isothermal Titration Calorimetry

ITC was performed using a VP ITC (MicroCal, Inc., Northampton, MA). All samples were pH 7.0 in 10 mM HEPES. Titrations were performed by injecting 30 consecutive 10 μl aliquots of ~200 μM TbpB (intact or N lobe) titrant into the ITC cell (volume = 1.3528 mL) containing ~15 μM holo-pTf (concentrations of the proteins were specifically determined by absorbance at 280 nm). The ITC data were corrected for the heat of dilution of the titrant by subtracting mixing enthalpies for 10 μl injections of TbpB into protein-free buffer. Binding stoichiometry, enthalpy, and equilibrium association constants were determined by fitting the corrected data to a bimolecular interaction model.

Multiangle Light Scattering

Purified protein (0.5 mg) was loaded onto a Superdex 200 HR 10/30 gel filtration column (Amersham), equilibrated with buffer (10 mM HEPES, 50 mM NaCl [pH 7.0]), and connected in line with miniDAWN MALS equipment coupled to an interferometric refractometer (Wyatt Technologies). Data analysis was carried out in real time using ASTRA (Wyatt Technologies), and molecular masses were calculated using the Debye fit method.

Accession Codes

Coordinates for $Ap\text{-}TbpB^{20-528}$ and $Ap\text{-}TbpB^{35-285}$ have been deposited in the Protein Data Bank under ID codes 3HOE and 3HOL.

SUPPLEMENTAL DATA

Supplemental Data include one table and seven figures and can be found with this article online at http://www.cell.com/molecular-cell/supplemental/S1097-2765(09)00467-5.

ACKNOWLEDGMENTS

We thank Stephen Shouldice and Colin Shima for preliminary protein expression studies and Louise Creagh and Ewa Poduch for assistance with ITC at UBC and U of T/OCI. We thank Bart Hazes for access to robotics and Igor D'Angelo and Canadian Light Source (CLS) beamline staff at CMCF-08ID-1 for assistance with data collection. This research was funded with operating and infrastructure support provided by Canadian Foundation for Innovation (CFI), the Alberta Heritage Foundation for Medical Research (AHFMR), the Michael Smith Foundation for Health Research (MSFHR), the Howard Hughes Medical Institute (HHMI), and the Canadian Institutes of Health Research (CIHR). N.C.J.S. is a MSFHR Senior Scholar, CIHR Investigator, and HHMI International Scholar, and T.F.M. was funded by a MSFHR fellowships.

Received: January 23, 2009
Revised: May 9, 2009
Accepted: June 11, 2009
Published: August 27, 2009

REFERENCES

Alcantara, J., Yu, R.H., and Schryvers, A.B. (1993). The region of human transferrin involved in binding to bacterial transferrin receptors is localized in the C-lobe. Mol. Microbiol. *8*, 1135–1143.

Anderson, J.E., Sparling, P.F., and Cornelissen, C.N. (1994). Gonococcal transferrin-binding protein 2 facilitates but is not essential for transferrin utilization. J. Bacteriol. *176*, 3162–3170.

Baker, N.A., Sept, D., Joseph, S., Holst, M.J., and McCammon, J.A. (2001). Electrostatics of nanosystems: application to microtubules and the ribosome. Proc. Natl. Acad. Sci. USA *98*, 10037–10041.

Baltes, N., Hennig-Pauka, I., and Gerlach, G.F. (2002). Both transferrin binding proteins are virulence factors in Actinobacillus pleuropneumoniae serotype 7 Infection. FEMS Microbiol. Lett. *209*, 283–287.

Cantini, F., Savino, S., Scarselli, M., Masignani, V., Pizza, M., Romagnoli, G., Swennen, E., Veggi, D., Banci, L., and Rappuoli, R. (2006). Solution structure of the immunodominant domain of protective antigen GNA1870 of Neisseria meningitidis. J. Biol. Chem. *281*, 7220–7227.

Cantini, F., Veggi, D., Dragonetti, S., Savino, S., Scarselli, M., Romagnoli, G., Pizza, M., Banci, L., and Rappuoli, R. (2009). Solution structure of the factor H-binding protein, a survival factor and protective antigen of Neisseria meningitidis. J. Biol. Chem. *284*, 9022–9026.

Cheng, Y., Zak, O., Aisen, P., Harrison, S.C., and Walz, T. (2004). Structure of the human transferrin receptor-transferrin complex. Cell *116*, 565–576.

Chimento, D.P., Kadner, R.J., and Wiener, M.C. (2003). The Escherichia coli outer membrane cobalamin transporter BtuB: structural analysis of calcium and substrate binding, and identification of orthologous transporters by sequence/structure conservation. J. Mol. Biol. *332*, 999–1014.

Cornelissen, C.N., Biswas, G.D., Tsai, J., Paruchuri, D.K., Thompson, S.A., and Sparling, P.F. (1992). Gonococcal transferrin-binding protein 1 is required for transferrin utilization and is homologous to TonB-dependent outer membrane receptors. J. Bacteriol. *174*, 5788–5797.

Cornelissen, C.N., Kelley, M., Hobbs, M.M., Anderson, J.E., Cannon, J.G., Cohen, M.S., and Sparling, P.F. (1998). The transferrin receptor expressed by gonococcal strain FA1090 is required for the experimental infection of human male volunteers. Mol. Microbiol. *27*, 611–616.

Craig, L., Volkmann, N., Arvai, A., Pique, M., Yeager, M., Egelman, E.H., and Tainer, J. (2006). Type IV pilus structure by cryo-electron microscopy and crystallography: implications for pilus assembly and functions. Mol. Cell *23*, 651–662.

Danve, B., Lissolo, L., Mignon, M., Dumas, P., Colombani, S., Schryvers, A.B., and Quentin-Millet, M.J. (1993). Transferrin-binding proteins isolated from Neisseria meningitidis elicit protective and bactericidal antibodies in laboratory animals. Vaccine *11*, 1214–1220.

DeLano, W. (2002). The PyMOL Molecular Graphics System (http://www.pymol.com).

Fanucci, G.E., Coggshall, K.A., Cadieux, N., Kim, M., Kadner, R.J., and Cafiso, D.S. (2003). Substrate-induced conformational changes of the periplasmic N-terminus of an outer-membrane transporter by site-directed spin labeling. Biochemistry *42*, 1391–1400.

Ferguson, A.D., Hofmann, E., Coulton, J.W., Diederichs, K., and Welte, W. (1998). Siderophore-mediated iron transport: crystal structure of FhuA with bound lipopolysaccharide. Science *282*, 2215–2220.

Gerlach, G.F., Anderson, C., Potter, A.A., Klashinsky, S., and Willson, P.J. (1992). Cloning and expression of a transferrin-binding protein from Actinobacillus pleuropneumoniae. Infect. Immun. *60*, 892–898.

Gonzalez, G.C., Caamano, D.L., and Schryvers, A.B. (1990). Identification and characterization of a porcine-specific transferrin receptor in *Actinobacillus pleuropneumoniae*. Mol. Microbiol. *4*, 1173–1179.

Gonzalez, G.C., Yu, R.H., Rosteck, P.R., and Schryvers, A.B. (1995). Sequence, genetic analysis, and expression of Actinobacillus pleuropneumoniae transferrin receptor genes. Microbiology *141*, 2405–2416.

Gray, J.J., Moughon, S., Wang, C., Schueler-Furman, O., Kuhlman, B., Rohl, C.A., and Baker, D. (2003). Protein-protein docking with simultaneous optimization of rigid-body displacement and side-chain conformations. J. Mol. Biol. *331*, 281–299.

Gray-Owen, S.D., and Schryvers, A.B. (1995). Characterization of transferrin binding proteins 1 and 2 in invasive type b and nontypeable strains of Haemophilus influenzae. Infect. Immun. *63*, 3809–3815.

Hendrickson, W.A., Smith, J.L., and Sheriff, S. (1985). Direct phase determination based on anomalous scattering. Methods Enzymol. *115*, 41–55.

Irwin, S.W., Averil, N., Cheng, C.Y., and Schryvers, A.B. (1993). Preparation and analysis of isogenic mutants in the transferrin receptor protein genes, tbpA and tbpB, from Neisseria meningitidis. Mol. Microbiol. *8*, 1125–1133.

Lawrence, C.M., Ray, S., Babyonyshev, M., Galluser, R., Borhani, D.W., and Harrison, S.C. (1999). Crystal structure of the ectodomain of human transferrin receptor. Science *286*, 779–782.

Madico, G., Welsch, J.A., Lewis, L.A., McNaughton, A., Perlman, D.H., Costello, C.E., Ngampasutadol, J., Vogel, U., Granoff, D.M., and Ram, S. (2006). The meningococcal vaccine candidate GNA1870 binds the complement regulatory protein factor H and enhances serum resistance. J. Immunol. *177*, 501–510.

Mascioni, A., Bentley, B., Camarda, R., Dilts, D., Fink, P., Gusarova, V., Hoiseth, S., Jacob, J., Lin, S., Malakian, K., et al. (2008). Structural basis for the immunogenic properties of the meningococcal vaccine candidate LP2086. J. Biol. Chem. *284*, 8738–8746.

Morris, R.J., Perrakis, A., and Lamzin, V.S. (2002). ARP/wARP's model-building algorithms. I. The main chain. Acta Crystallogr. D Biol. Crystallogr. *58*, 968–975.

Murshudov, G., Vagin, A., and Dodson, E. (1997). Refinement of macromolecular structures by the maximum-likelihood method. Acta Crystallogr. D Biol. Crystallogr. *53*, 240–255.

Myers, L.E., Yang, Y.P., Du, R.P., Wang, Q., Harkness, R.E., Schryvers, A.B., Klein, M.H., and Loosmore, S.M. (1998). The transferrin binding protein B of Moraxella catarrhalis elicits bactericidal antibodies and is a potential vaccine antigen. Infect. Immun. *66*, 4183–4192.

Otwinowski, Z., and Minor, W. (1997). Processing of X-ray diffraction data collected in oscillation mode. Methods Enzymol. *276*, 307–326.

Potter, A.A., Schryvers, A.B., Ogunnariwo, J.A., Hutchins, W.A., Lo, R.Y., and Watts, T. (1999). Protective capacity of the Pasteurella haemolytica transferrin-binding proteins TbpA and TbpB in cattle. Microb. Pathog. *27*, 197–206.

Ratledge, C., and Dover, L.G. (2000). Iron metabolism in pathogenic bacteria. Annu. Rev. Microbiol. *54*, 881–941.

Rawas, A., Muirhead, H., and Williams, J. (1997). Structure of apo duck ovotransferrin: the structures of the N and C lobes are in the open form. Acta Crystallogr. D Biol. Crystallogr. *53*, 464–468.

Renauld-Mongénie, G., Poncet, D., von Olleschik-Elbheim, L., Cournez, T., Mignon, M., Schmidt, M.A., and Quentin-Millet, M.J. (1997). Identification of human transferrin-binding sites within meningococcal transferrin-binding protein B. J. Bacteriol. *179*, 6400–6407.

Renauld-Mongénie, G., Lins, L., Krell, T., Laffly, L., Mignon, M., Dupuy, M., Delrue, R.M., Guinet-Morlot, F., Brasseur, R., and Lissolo, L. (2004). Transferrin-binding protein B of Neisseria meningitidis: sequence-based identification of the transferrin-binding site confirmed by site-directed mutagenesis. J. Bacteriol. *186*, 850–857.

Retzer, M.D., Yu, R., Zhang, Y., Gonzalez, G.C., and Schryvers, A.B. (1998). Discrimination between apo and iron-loaded forms of transferrin by transferrin binding protein B and its N-terminal subfragment. Microb. Pathog. *25*, 175–180.

Retzer, M.D., Yu, R.H., and Schryvers, A.B. (1999). Identification of sequences in human transferrin that bind to the bacterial receptor protein, transferrin-binding protein B. Mol. Microbiol. *32*, 111–121.

Rokbi, B., Mignon, M., Maitre-Wilmotte, G., Lissolo, L., Danve, B., Caugant, D.A., and Quentin-Millet, M.J. (1997). Evaluation of recombinant transferrin-binding protein B variants from Neisseria meningitidis for their ability to induce cross-reactive and bactericidal antibodies against a genetically diverse collection of serogroup B strains. Infect. Immun. *65*, 55–63.

Rossi-Campos, A., Anderson, C., Gerlach, G.F., Klashinsky, S., Potter, A.A., and Willson, P.J. (1992). Immunization of pigs against Actinobacillus pleuropneumoniae with two recombinant protein preparations. Vaccine *10*, 512–518.

Schneider, M.C., Prosser, B.E., Caesar, J.J., Kugelberg, E., Li, S., Zhang, Q., Quoraishi, S., Lovett, J.E., Deane, J.E., Sim, R.B., et al. (2009). Neisseria meningitidis recruits factor H using protein mimicry of host carbohydrates. Nature *458*, 890–893.

Schryvers, A.B., and Morris, L.J. (1988). Identification and characterization of the transferrin receptor from Neisseria meningitidis. Mol. Microbiol. *2*, 281–288.

Sebunya, T.N., and Saunders, J.R. (1983). Haemophilus pleuropneumoniae infection in swine: a review. J. Am. Vet. Med. Assoc. *182*, 1331–1337.

Sims, K.L., and Schryvers, A.B. (2003). Peptide-peptide interactions between human transferrin and transferrin-binding protein B from Moraxella catarrhalis. J. Bacteriol. *185*, 2603–2610.

Strutzberg, K., von Olleschik, L., Franz, B., Pyne, C., Schmidt, M.A., and Gerlach, G.F. (1995). Mapping of functional regions on the transferrin-binding protein (TfbA) of Actinobacillus pleuropneumoniae. Infect. Immun. *63*, 3846–3850.

Strutzberg, K., Franz, B., and Gerlach, G.F. (1997). Interference of peptides and specific antibodies with the function of the Actinobacillus pleuropneumoniae transferrin-binding protein. Infect. Immun. *65*, 5346–5348.

Vonrhein, C., Blanc, E., Roversi, P., and Bricogne, G. (2007). Automated structure solution with autoSHARP. Methods Mol. Biol. *364*, 215–230.

Winn, M., Isupov, M., and Murshudov, G. (2001). Use of TLS parameters to model anisotropic displacements in macromolecular refinement. Acta Crystallogr. D Biol. Crystallogr. *57*, 122–133.

Yu, R.H., and Schryvers, A.B. (1993). The interaction between human transferrin and transferrin binding protein 2 from Moraxella (Branhamella) catarrhalis differs from that of other human pathogens. Microb. Pathog. *15*, 433–445.